Asymmetric Oxidation of Giant Vesicles Triggers Curvature-Associated Shape Transition and Permeabilization

Julien Heuvingh[†*] and Stéphanie Bonneau[‡*]

[†]Université Paris Diderot, Laboratoire de Physique et Mécanique des Milieux Hétérogènes, UMR7636, Centre National de la Recherche Scientifique/Ecole Superieure Physique Chimie Industrielles Ville de Paris, Université Pierre et Marie Curie, Paris, France; and [‡]Université Pierre et Marie Curie, Laboratoire Acides Nucleiques et Biophotonique, FRE3207, Centre National de la Recherche Scientifique, Paris, France

ABSTRACT Oxidation of unsaturated lipids is a fundamental process involved in cell bioenergetics as well as in cell death. Using giant unilamellar vesicles and a chlorin photosensitizer, we asymmetrically oxidized the outer or inner monolayers of lipid membranes. We observed different shape transitions such as oblate to prolate and budding, which are typical of membrane curvature modifications. The asymmetry of the shape transitions is in accordance with a lowered effective spontaneous curvature of the leaflet being targeted. We interpret this effect as a decrease in the preferred area of the targeted leaflet compared to the other, due to the secondary products of oxidation (cleaved-lipids). Permeabilization of giant vesicles by light-induced oxidation is observed after a lag and is characterized in relation with the photosensitizer concentration. We interpret permeabilization as the opening of a pore above a critical membrane tension, resulting from the budding of vesicles. The evolution of photosensitized giant vesicle lysis tension was measured and yields an estimation of the effective spontaneous curvature at lysis. Additionally photo-oxidation was shown to be fusogenic.

INTRODUCTION

The oxidation of unsaturated lipids is of great interest, both from the biological and medical points of view (1–5). It may be generated in enzymatic or nonenzymatic reactions involving short-lived activated chemical species known as reactive oxygen species (ROS) (6). In cells, ROS are generated during the normal respiration process involving oxygen, oxidases, and electron transport in mitochondria or the endoplasmic reticulum. Peroxidation of unsaturated lipids may be responsible, in vivo, for pathological processes such as drug-induced phototoxicity, arthrosclerosis, and aging (3,4). At cellular level, oxidation of lipids is involved in dysfunctions such as enhanced permeability, changes in membrane fluidity, or release of lysosomal enzymes. In addition, the presence of oxidized phospholipids in lipidic membranes induces changes in their physical properties (7,8).

The photochemical induction of oxidation is an effective way of inducing oxidation processes (6). It is supported by the ability of certain molecules, called photosensitizers, to generate ROS upon light irradiation. The specificity and preferential retention of certain photosensitizers by tumors, as compared to normal surrounding tissues, are the basis of an anti-tumoral therapy, i.e., photodynamic therapy (9). Used at high level, such light-induced molecular damage leads to the targeted cell's death. More recently, photosensitizer-induced lipid oxidation has been used to deliver macromolecular therapeutic agents to their intracellular targets by an approach called photochemical internalization (10). After the uptake by endocytosis, the degradation of the macromolecules in lysosomes is greatly reduced by the photodynamic destabilization of the endocytic vesicles membrane, increasing their biological activity.

The short half-life and limited diffusion length of the photo-induced ROS necessitate the close association of photosensitizers with the target site. For example, chlorin-generated subcellular singlet oxygen lifetime has been experimentally measured between 4.5 $\pm$ 0.5 μs and 17 $\pm$ 2 μs (11). ROS typically diffuse <0.1 μm in a biological environment (12,13). Due to the localized action of photosensitizers, the characteristics of their interaction with lipidic membranes are an important parameter controlling the effects of the photosensitizer-induced lipid oxidation (14). For tetrapyrrole photosensitizers, the ability to cross membranes is governed by the charge of their lateral chains (15–17). The chlorin e6 (Ce6), a second-generation photosensitizer, is not able to cross the biological membranes (18,19). This allows an asymmetric labeling of the membrane, where the photosensitizer interacts only with the monolayer in contact with the photosensitizer solution. We thus labeled the model membranes—giant unilamellar vesicles (GUVs), composed of dioleoylphosphatidylcholine, an unsaturated lipid. Under light-induced oxidation, we observed morphological transitions and permeation of the GUVs.

Morphological transitions in GUVs have previously been observed in response to pH difference between compartments (20,21), change in temperature (22), grafting of polymers on the membrane (23), ion adsorption on the lipid heads (24), or photoisomerization of azobenzene-containing amphiphiles (25). One of the first models to account for various morphologies in vesicles was the spontaneous curvature model introduced by Helfrich (26). Increasing the spontaneous curvature induces membrane budding outside the GUVs, whereas a decrease of the spontaneous curvature down to negative

Submitted January 23, 2009, and accepted for publication August 17, 2009.

*Correspondence: julien.heuvingh@espci.fr or stephanie.bonneau@upmc.fr

Editor: Joshua Zimmerberg.

0006-3495/09/12/2904/9 $2.00

doi: 10.1016/j.bpj.2009.08.056

values induces a stomatocyte shape or budding inside the vesicle. Refinement of the theoretical comprehension of vesicle shape transitions led to the area-difference elasticity (ADE) model, which takes into account the area difference between the two monolayers (27,28). Any vesicle can then be defined by an area/volume ratio and a term of effective spontaneous curvature, which contains the area difference between the monolayers and the spontaneous local curvature. These two parameters give a phase diagram of vesicle shape that has been explored (22). For area/volume ratio corresponding to nearly spherical vesicles, an increase of the effective spontaneous curvature leads to shape transitions from an oblate ellipsoid to a prolate ellipsoid, and then to a pear-shape and to a budding vesicle. Reducing the effective spontaneous curvature leads to a stomatocyte shape or inside budding.

DOPC membranes are essentially water-permeable (40 μm/s (29)), but they are impermeable to polar solutes such as sugar at the time-length involved in these experiments (6 10^{-5} μm/s (30)). Due to osmotic equilibrium, the very slow permeability ensures a constant volume for vesicles. A much higher solute permeability is possible via pores, holes in the membrane allowing free flow. These pores have been observed in GUVs (31,32). They are energetically unfavorable because of the high cost of the exposition to water of hydrophobic lipid tails at the rim of the pore (33,34).

In this work, we photochemically induce the lipid oxidation in DOPC-GUVs. The photosensitizer used, Ce6, allows a symmetric as well as an asymmetric targeting of the membrane bilayers and a fine control of the location of the oxidation. The induced morphological transitions are correlated to the targeted leaflet and show a decrease in the spontaneous curvature of the targeted leaflet. The eventual permeabilization of the membrane has been measured and can be linked to the tension from the budding of vesicles.

MATERIALS AND METHODS

Chemicals

All chemicals were purchased from Sigma (St. Louis, MO), except dioleoylphosphatidylcholine (DOPC) and dipalmitoylphosphatidylcholine (DPPC) from Avanti Polar Lipids (Alabaster, AL), and chlorin e6 from Porphyrin Products (Frontier Scientific, Logan, UT). Chlorin stock solution (5 mM) was prepared in ethanol and kept at −18°C. The experimental Ce6 aqueous solutions were prepared, used immediately, and handled in the dark. The osmolarity of the solutions was checked with an osmometer (Roebling Osmometer, Berlin, Germany).

GUV formation

GUVs were formed by the electroswelling method (35). DOPC in chloroform was deposed on ITO-covered glass plates. A chamber was made from two such glass plates and a Teflon spacer of 4 mm; the solvent was dried in vacuum. The chamber was filled then with a solution of 300 mM sucrose and an AC field of 1 Volt and 8 Hz was applied between the plates for 4 h. For DOPC versus DPPC comparison, electroformation took place at 50°C, above the transition temperature of DPPC.

For observation, the GUVs were mixed with a 300 mM glucose solution. The density difference between sucrose and glucose caused the GUVs to sediment to the bottom of the chamber. The difference in optical index between sucrose inside and glucose outside the vesicle allowed phase contrast microscopy observation.

Chlorin labeling

GUVs were asymmetrically labeled with chlorin. The chlorin molecules were present outside the vesicles, inside the vesicles or both outside and inside. The concentrations of chlorin used were 2.5, 5, 12.5, 25, 50, and 125 μM. The measured pH of the solutions was 5.1 $\pm$ 0.2. For chlorin present outside the vesicles, chlorin was diluted in the glucose solution before mixing with GUVs. For chlorin present inside the vesicles, GUVs were prepared with a sucrose solution containing chlorin in the chamber and subsequently rinsed. Rinsing was achieved by mixing the GUVs with the glucose solution and carefully centrifuging them twice (25 *g* for 20 min). At the typical lipid concentration in the GUV solution (~10^{-6} M), the majority of the chlorin is unbound. This fact, combined with the high exchange rate of the chlorin with the bulk medium (19) ensures the exit of the sensitizer from the membrane outer leaflet and its rinsing. GUVs with symmetrical chlorin distribution were prepared with a sucrose solution containing chlorin in the chamber and then mixed with a chlorin-containing glucose solution.

Observation and illumination

GUVs were observed under an Eclipse TE2000-U inverted microscope equipped with a 1.3 NA 100× oil objective (Nikon, Melville, NY). Illumination was provided by a 100 W Hg-arc lamp with a 465–495 nm bandpass filter. Images were acquired with a model No. A602f digital camera (Basler Vision Technologies, Ahrensburg, Germany) using LABVIEW (National Instruments, Austin, TX). Images were analyzed using IMAGE J (National Institutes of Health, Bethesda, MD) and SCILAB (l'Institut National de Recherche en Informatique, Sophia Antipolis, France; www.scilab.org).

Tension measurement

Micropipettes were made from borosilicate glass capillary GC100-15 tubing (1.0-mm outside diameter × 0.58-mm wall thickness × 7-cm length; Harvard Apparatus, Kent, UK) using a pipette puller (model No. P-2000; Sutter Instruments, San Rafael, CA). A homemade microforge was used to tune their inner diameter from 2.3 to 5.3 μm. Pipettes were coated with bovine serum albumin and rinsed extensively. Before experiments, the pipettes were filled with the glucose solution. A suction pressure was applied in the pipette by hydrostatic pressure. The suction pressure P produces a tension τ in the membrane such as

$$\tau = P.D_P/4(1 - D_P/D_V), \quad (1)$$

where D_P and D_V are, respectively, the diameters of the pipette and of the vesicle (33).

Statistics

Correlation between the radius and permeabilization time of vesicle were analyzed by a *t*-test on the regression analysis with a statistical significance of 0.01. When the two parameters correlated, the time was corrected, i.e., deduced from the regression using a radius of 3.98 μm, which is the mean GUV radius of our samples. When no correlation was found, the average over the vesicles was simply used.

RESULTS

Shape transitions

We prepared GUVs with different localizations of chlorin e6 regarding the leaflets. As chlorin molecules have a high

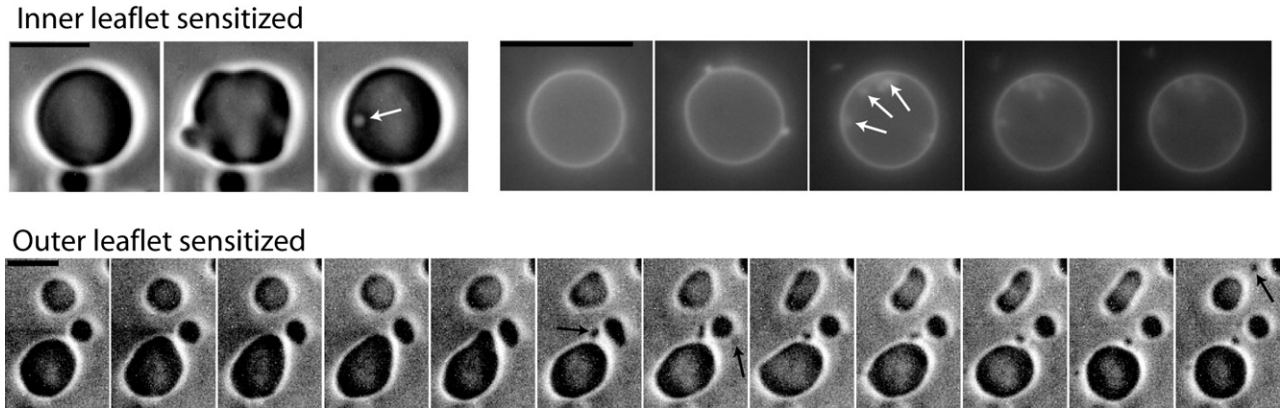

FIGURE 1 Time sequences of giant vesicles with photosensitizers targeted to the outer leaflet (*upper row*) or to the inner leaflet (*lower row*). The bar is 10 μm; the time lapse between two images is 1 s. In the first sequence of the upper row (*phase contrast microscopy*), a GUV photosensitized in its outer leaflet endures a short-time deformation (*second image*) followed by a budding toward the inside (*open arrow*). In the second sequence of the upper row (fluorescence of chlorin), a GUV photosensitized in its outer leaflet endures a deformation (*second image*) followed by multiple budding toward the inside (*open arrows*). In the sequence of the lower row (*phase contrast microscopy*), three GUVs photosensitized in their inner leaflet show deformations: the upper vesicle exhibits a transition from oblate to prolate (due to the projection, oblate appears as *circle* and prolate as *ellipse*), whereas the two other vesicles are deformed into pear shapes. These shape transitions are followed by a budding to the outside on each GUV (*solid arrows*). The morphology transitions observed when the outer leaflet is targeted denote a decrease of the membrane's equivalent curvature, whereas those observed when the inner leaflet is targeted denote an increase of the membrane's equivalent curvature.

affinity for lipids and do not flip-flop at the timescale involved in these experiments (18,19), Ce6 labels only the leaflet directly in contact with the photosensitizer solution. Thus, GUVs labeled with Ce6 in the outer, the inner, and both leaflets, were studied.

Upon illumination, all vesicles containing photosensitizers underwent major shape transitions within a few to a hundred seconds after illumination start (see Fig. 1). Vesicles with photosensitizer in the inner leaflet showed shape transitions from oblate to prolate ellipsoids, pear-shape deformations, and budding of small vesicles outside the GUVs. Vesicles in the prolate shape fluctuated during tens of seconds until the budding of vesicles put them out of prolate shape. Vesicles with photosensitizer in the outer leaflets typically showed deformation for a short time ($<$2 s) followed by an invagination or budding of a small vesicle inside the GUVs. The budded vesicles were visible as light dots contrasting with the GUV inner medium. Vesicles with Ce6 in both leaflets show all of the above-mentioned shape transitions. Finally, vesicles with no Ce6 showed none of these shape transitions for $>$15 min. A quantification of these shape transitions is presented in Fig. 2. These results are in accordance with a lowered spontaneous curvature of the leaflet in which photo-oxidation occurs.

Permeabilization

Vesicles with chlorin in the outer or both leaflets undergo permeabilization. The contrast between the vesicle and the surrounding solution gradually fades away until there is no phase difference between inside and outside medium and the vesicle is barely observable by its membrane. This is a signature of the sucrose diffusion from the inner medium to the outer medium and its replacement by glucose from the outer medium (36). A small portion of the vesicles ($<$10%) burst or leaked abruptly in a nongradual fashion. We quantified the contrast fading, which typically varies like a decreasing exponential (Fig. 3, *left*)

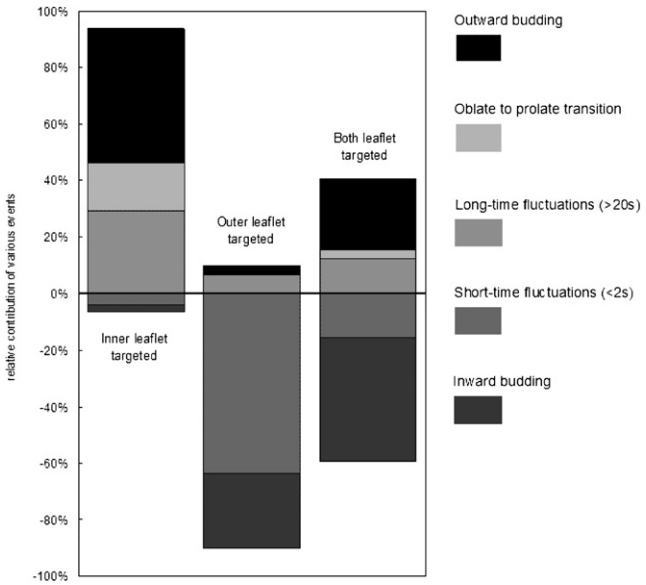

FIGURE 2 Proportion of each type of photoinduced morphology transition as a function of photosensitizer localization. (*Top* to *bottom*) Outward budding (*open dots* on *solid*), oblate to prolate transition (*close dots*), long-time fluctuations ($>$20 s) (*spaced dots*), short-time fluctuations ($<$2 s) (*wide hatching*), and inward budding (*close hatching*). The midline between long- and short-time fluctuations materializes the separation between events associated with an increase of the effective spontaneous curvature (*above the line*) and those associated with a decrease of the effective spontaneous curvature (*below the line*).

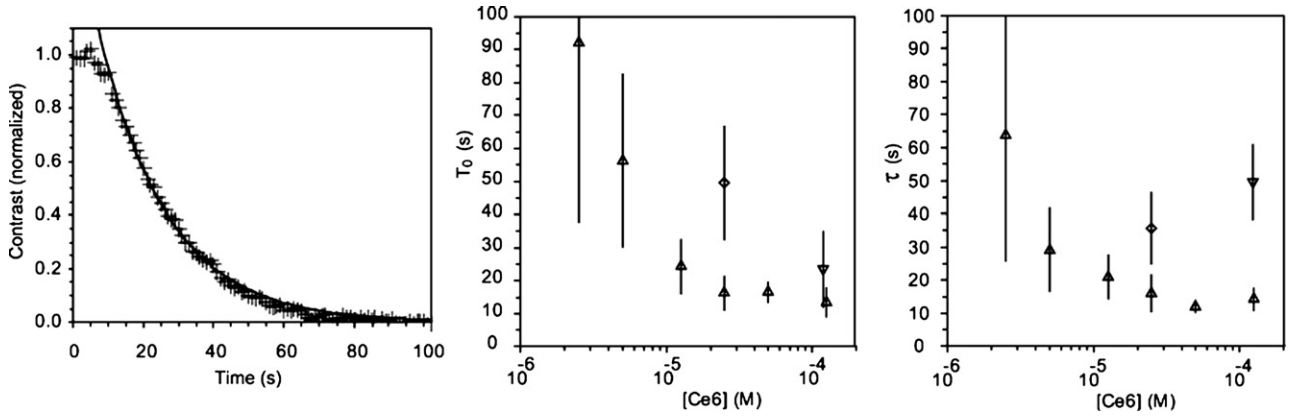

FIGURE 3 Permeabilization of vesicles. (*Left*) Typical evolution of the contrast between the inside and outside of a photosensitized vesicle at 25 μM Ce6 in the outer medium. The decay of the contrast shows equilibrium between the inside solute (sucrose) and the outside solute (glucose). The experimental points are fitted by a decreasing exponential, from which are extracted a starting and a characteristic time of permeabilization. (*Center* and *right*) Starting time (t_0) and characteristic time (τ) of permeabilization for 50–120 vesicles for each concentration of Ce6. (*Upward triangles*) Vesicles with Ce6 in the outer medium; (*downward triangles*) vesicles with Ce6 in the inner medium; and (*diamonds*) in both media. The dependence on the vesicle radius is corrected (for τ at all concentrations and for t_0 at 50- and 125-μM outer medium).

$$\boldsymbol{c} = \boldsymbol{c}_0 \exp(-(t - t_0)/\tau), \quad (2)$$

where $\boldsymbol{c}$ is the concentration of sucrose in the inner medium, $\boldsymbol{c}_0$ its initial concentration, t_0 the initial time of the experiment, and τ the characteristic time of the diffusion process.

In accordance with Eq. 2, we extracted a starting and a characteristic leaking time. The exponential fit is in good agreement with the data ($R_2 > 0.95$ for >87% of the vesicles and $R_2 > 0.9$ for >96% of the vesicles). The characteristic and starting times were compared with the vesicle radius. The starting time is statistically independent of the vesicle size, except at the highest concentration of Ce6 (50 and 125 μM outside the vesicle). The characteristic time depends on the vesicle radius at all concentrations. The dependence is stronger for high concentrations than for low ($R^2 = 0.69$ for 125 μM, $R^2 = 0.22$ for 2.5 μM).

The starting and characteristic permeabilization times decrease when the quantity of chlorin is increased for GUVs with photosensitizers in the outer medium (Fig. 3, *right*). A plateau is evidenced over 25 μM. The permeabilization is slower for vesicles photosensitized on both leaflets. In the case of vesicles with photosensitizer only in the inner medium, vesicles are not permeabilized after 15 min, except for the higher concentration of 125 μM. At this concentration, permeabilization is three times longer for vesicles bearing Ce6 on their inner leaflet than for vesicles bearing Ce6 on their outer leaflet. All vesicles had a spherical shape (showing tension) before the start of permeabilization.

To verify that the permeabilization was mainly due to the oxidation of the lipid unsaturation, we compared the photosensitization effect on DOPC and DPPC, which is a saturated phospholipid. The experiment was conducted at 50°C, above the transition temperature of DPPC. The vesicles were in presence of 25 μM Ce6 and illuminated by a 100 W Hg-arc lamp during 2 s without any filter. Contrary to the DOPC-GUVs, the DPPC-GUVs did not permeabilize for >5 min (see Fig. S1 in the Supporting Material). The DOPC-GUVs lost half of their contrast in 44 s ± 25 s, whereas >70% of the DPPC-GUVs retained more than half of their contrast 300 s after illumination. No systematic shape changes were detected with DPPC-GUVs.

Lysis tension

Micropipette experiments were conducted to estimate the lysis tension of photosensitized DOPC-GUVs. Vesicles in the presence of 50 μM Ce6 in the outer medium were held by a micropipette and a suction pressure between 50 and 500 Pascal was applied, corresponding to a membrane tension from 0.05 to 0.5 mN/m (see Materials and Methods). We kept the vesicle's tension constant and illuminated the sample. After a few seconds of illumination the vesicle's integrity was compromised, i.e., it disappeared inside the pipette. This is interpreted as the opening of a hole in the membrane, allowing the inside solution to leave the vesicle and the membrane to be sucked inside the pipette. The time between illumination and permeabilization was recorded and is presented in Fig. 4. It can be thought as the evolution of lysis tension over time. The time at which the vesicles permeabilize in experiments without pipettes is plotted on the same graph. This time corresponds to the time at which vesicles tensed at 0.15 mN/m leaked. Vesicles tensed in presence of Ce6 without illumination did not break for several minutes.

Fusion

Fusion of giant vesicles in contact with each other occurred frequently for GUVs of >10 μm radius at the highest concentrations (125 μM) in outer leaflets. The contacts between these GUVs lead to fusion in 71% of the cases (35 fusion events). See Movie S1 in the Supporting Material.

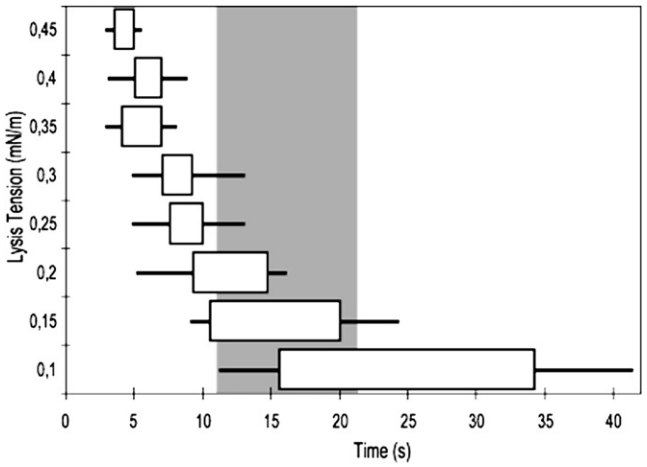

FIGURE 4 Evolution of lysis tension over time during photodamage. The time after the start of the illumination at which lysis occurs was recorded for different membrane tensions (113 vesicles total). The boundaries of the boxes are the upper and lower quartiles (median 50% *inside the box*). The whiskers boundaries are the upper and lower deciles (median 80% *inside the whisker*).

We observed <5% of fusion between vesicles of <10 μm radius at 50 μM Ce6 and below. A more precise quantification of fusion proved difficult, as the number of contacts is highly dependent on the size and density of the vesicle preparation. After micropipette experiments, when the vesicles were gradually aggregated by the evaporation in the experimental chamber, fusion occurred at a dramatically accelerated rate when illuminated.

DISCUSSION

Photo-oxidation products

The chlorin e6 is a photosensitizer: it interacts very efficiently with light to produce reactive species (singlet oxygen and radicals) from its long-life triplet state. In ethanol, its quantum yield for $^1O_2$ production is important (at ~0.65 (37)). In unsaturated lipids, excitation of a photosensitizer generates peroxides (38), which are highly unstable in the presence of any trace of transition metal (39). In our microscopy experiments, it will spontaneously decay to a free radical lipid, which pulls out a hydrogen from another unoxidized unsaturated lipid, creating a new free radical and a hydroxylated lipid. The combination of molecular oxygen with the new free radical leads again to the removing of a hydrogen from another lipid and produces, again, free radical and lipid peroxide. The lipid peroxidation is thus a radical chain-reaction leading to the formation of intermediate hydroperoxide (Fig. 5). The hydroperoxyl group induces hydrophilicity in the chains of lipids.

If it remains in the hydrocarbon region of the membrane bilayer, the hydroperoxyl group should drastically change the membrane architecture by increasing the cross-section area of its lipid tails. The peroxide lipid would therefore

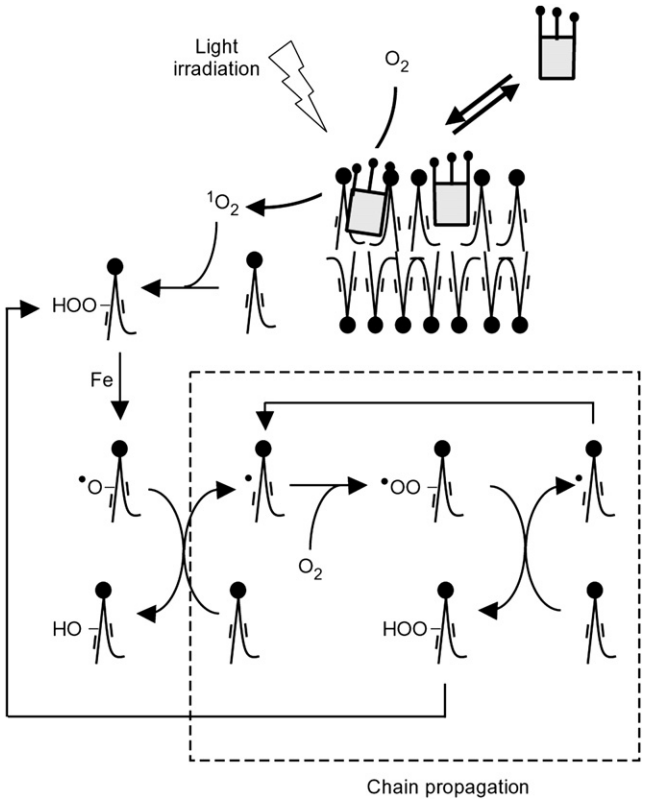

FIGURE 5 Diagram of the lipid photo-oxidation processes in the vesicle membrane. The lipid oxidation, initiated via singlet oxygen, is a chain reaction.

have a packing parameter >1 and would increase the relaxed area of the leaflet in which they are present. However, indirect evidences on polyunsaturated lipids have suggested that the peroxide group may more likely be near the water/membrane interface (40). In this case, the peroxide lipid will have a packing parameter <1 and will still increase the leaflet relaxed area. Additionally, in presence of trace amounts of catalytic transition metals (e.g., Fe^{2+}), the photo-oxidation of biological lipidic systems results in a myriad of secondary products (39,41). For monounsaturated fatty acids (like the hydrocarbon chains of DOPC), these major final products correspond to the cleavage of the carbon chain near the initial position of the double bound and give an alkene or an aldehyde (41). Such cleaved-lipids present a strongly modified geometry as compared to DOPC. They correspond to a packing parameter <1 and to a decrease of the relaxed area in the leaflet in which they are present. They are also known to favor pore formation (33).

Changes in effective spontaneous curvature

The light-induced shapes observed in the vesicles containing photosensitizer in the inner leaflet (prolate, pears, external budding) correspond to shapes of higher effective spontaneous curvature in the ADE model. The large and slow fluctuations observed in this case are also typical of an increase

of the effective spontaneous curvature near the budding transition (42). The internal budding observed when the photosensitizer is in the outer leaflet corresponds to a lower effective spontaneous curvature. The variety of shape transitions observed is, therefore, qualitatively in accordance with a lowered effective spontaneous curvature of the leaflet, which is photosensitized.

More precisely, the effective spontaneous curvature in the ADE model is composed of two terms that cannot be experimentally separated. The first is the spontaneous curvature of the lipids linked to their packing parameter; the second is the difference in area between the two leaflets. Increasing the area of the external leaflet or changing its lipids toward cone shapes will increase the effective spontaneous curvature, whereas decreasing the area of the external leaflet or changing its lipids toward inverted cone shapes will decrease the effective spontaneous curvature. The effect on the membrane effective spontaneous curvature will be inversed if the internal leaflet is changed.

The products of lipid peroxidation discussed above will have contradicting effects on the effective spontaneous curvature of the leaflet. Lipid peroxides, whereas having a negative packing spontaneous curvature, will raise the leaflet effective spontaneous curvature by increasing its area. Inversely, cleaved-lipids have a positive packing spontaneous curvature but will lower the leaflet effective spontaneous curvature by decreasing its area. We need to estimate the magnitude of these effects on GUV membranes.

The effective spontaneous curvature can be expressed in the ADE model as

$$C_0^* = C_0 + \frac{\alpha\pi}{h}\frac{\Delta A_0}{A}, \tag{3}$$

where α is the ratio between the local and nonlocal bending rigidity, h is the thickness of a leaflet, C_0* and C_0 are, respectively, the effective spontaneous curvature of the membrane and the spontaneous curvature, and ΔA_0 is the optimal area difference between the two monolayers and A is the area of the membrane (28).

To compare the effect of lipid geometry on leaflet area increase, we use a simple geometric model, in which the cross-section area is increased from A/N to $(A + A_0)/\mathrm{N}$ at the position of the lipid double bond (N is the number of lipids in a leaflet). The spontaneous curvature of this lipid will then be equal to

$$C_0 = -\frac{1}{h}\frac{\Delta A_0}{A} \tag{4}$$

and the effective spontaneous curvature to

$$C_0^* = \frac{-1}{h}\frac{\Delta A_0}{A}. \tag{5}$$

This curvature is positive if ΔA_0 is positive for DOPC as $\alpha = 1.2$ (22). The area increase is therefore dominant over the lipids packing spontaneous curvature.

The formation of lipid peroxide consequently increases the leaflet effective spontaneous curvature. This is true whether the peroxide is located at the water/membrane interface or in the membrane bulk. Likewise, the formation of cleaved-lipids will decrease the leaflet effective spontaneous curvature. Although both of these chemical products will likely be present in the photosensitized membrane, our results indicate that the cleaved-lipids have the dominant effect on membrane spontaneous curvature, triggering the morphological transitions described here.

Permeabilization

Permeabilization of photosensitized GUVs was observed via the contrast fading as sucrose left the vesicle interior. The sucrose flux through a circular opening in the membrane is

$$\Phi_v = 2Ds\boldsymbol{c}, \tag{6}$$

where D is the diffusion coefficient of sucrose, s the radius of the aperture, and $\boldsymbol{c}$ the concentration in the inner medium (see Eq. 2) (34,38). We assumed the external sucrose concentration to be zero, as the internal volume is negligible compared to the outer volume. The concentration in the inner medium obeys $d\boldsymbol{c} = \Phi_v\, dt\, /V$ (V is the volume of the vesicle) and decreases exponentially with a characteristic time of $V/2Ds$.

The experimental data from the permeabilizations of individual GUVs are indeed well fitted by such a decreasing exponential, as shown in Fig. 3. The facts that permeabilization occurs suddenly, after 20–100 s of exposition, and after exponential decay in sucrose concentration, are both in good agreement with a pore-opening scenario. Based on the above model, the diameter of a pore is estimated to be between 16 nm and 43 nm for a typical vesicle (τ between 10.4 s and 27.5 s for a chlorin concentration above 12.5 μM; $R = 4\ \mu$m). These pore sizes are in the same range as the ones measured in electroporation of red blood cell ghosts (43) or the ones calculated for stretched giant vesicles (44).

Permeabilization and tension

Permeabilization and formation of a pore can be triggered by membrane tension. Membrane tension can be described as the combination of two contributions: an entropic tension due to the damping of thermal fluctuation modes, and an elastic term coming from the increased distance between the lipids. When measuring the area variation of a GUV while increasing the membrane tension (via micropipettes), these two contributions are visible successively. First, the membrane entropic ruffles are smoothed, corresponding to a soft exponential rise in area, then the membrane stretches, corresponding to a linear increase of area (45). Eventually the stretching will break the membrane above a critical stress. The lysis stress for DOPC-GUVs was measured to be 9.9 $\pm$ 2.6 mN/m (29). Unsurprisingly, photo-oxidation lowers the critical stress of DOPC vesicles as shown in our

experiments. We observe that the mean time of membrane rupture during photo-oxidation decreases when the tension is increased, which is interpreted as a reduction of lysis tension with the photo-oxidation duration. The starting time of vesicle permeabilization when no suction is externally applied corresponds to a lysis tension of 0.15 mN/m. Therefore, we hypothesize that when no external tension is applied, the vesicle tenses itself up to a tension of 0.15 ± 0.05 mN/m at which it lyses. We will show in the next paragraph how this tension can be reached through shape transition and budding. The fact that it takes longer for a vesicle to lyse when an external tension <1 mN/m is applied can be explained by a partial suppression of budding due to this preexisting tension (46). Interestingly, the measured lysis tension of 0.15 mN/m corresponds to the transition between thermal smoothing and stretching (see Fig. 2 in (45)), i.e., lysis occurs at the slightest stretching.

Budding and tension

In our experiments, the lipid oxidation on a GUV's external leaflet triggers a shape transition from a prolate form to a closed stomatocyte or internal budding. The volume/area ratio of the vesicle after internal budding will be that of a sphere. The ADE model, describing shape transitions due to curvature modifications, assumes the area to be constant and does not take into account any stretching of the membrane. Such description is perfectly valid for moderate changes in the curvature. However, above a certain level of curvature, the energy released from the budding will become important compared to the energy in the thermal fluctuations of the membrane. The vesicle would then be able to bud by tensing itself and taking area from the ripples of the membrane. We compare these two energies, in a manner similar to Glassinger and Raphael (47), to estimate the minimum effective spontaneous curvature required to tense the vesicle up to its lysis tension σ.

The energy gained when budding a vesicle of radius r from a vesicle of radius R ($r << R$) is

$$H_b = 8\pi k_c\left(1 - C_0^* r\right), \tag{7}$$

where k_c is the bending rigidity of the membrane (see detailed calculation in the Appendix).

The energy necessary to entropically stretch a membrane from a tension σ_0 to a tension σ is

$$H_S = A\frac{k_B T}{8\pi k_c}(\sigma - \sigma_0), \tag{8}$$

where A is the area of the giant vesicle, and k_B is the Boltzmann constant.

According to our hypothesis, the area gain from thermal fluctuation will be equal to the area of the budding vesicle:

$$\Delta A_{fluct} = A\frac{k_B T}{8\pi k_c} Ln\left(\frac{\sigma}{\sigma_0}\right) = 4\pi r^2. \tag{9}$$

Thus,

$$\sigma_0 = \sigma \exp\left(-\frac{8\pi k_c}{k_B T}\frac{r^2}{R^2}\right). \tag{10}$$

For small buds ($r << R\ (8\pi k_c/k_B T)^{1/2}$ ~250 nm), the stretching energy simplifies to

$$H_s = 4\pi r^2 \sigma. \tag{11}$$

The total energy is then given by

$$H = H_b + H_S = 4\pi r^2\sigma + 8\pi k_c\left(1 - C_0^* r\right). \tag{12}$$

It will be minimum for $r = k_c C_0^*/\sigma$, at which

$$H = 8\pi k_c\left(1 - C_0{}^{*2}\, k_c/2\sigma\right). \tag{13}$$

Budding will therefore be favorable for $C_0^* > (2\sigma/k_c)^{1/2}$.

Therefore, budding can be responsible for the vesicle's tension increase up to the observed lysis tension of 0.15 ± 0.05 mN/m, if the effective spontaneous curvature is >42 μm^{-1} (± 19 μm^{-1}). Expressed in terms of area difference, this corresponds to a decrease of 2.3% (± 1.1%) of one monolayer area as compared to the other.

It is tempting to explain the different permeabilization behavior between GUVs photosensitized on their outer or inner leaflet by the difference between external and internal budding. Due to external budding, GUVs photosensitized on their inner leaflet will lose both area and volume, whereas GUVs photosensitized on their outer leaflet will lose area and gain volume due to internal budding. This will result in more stretching when the outer leaflet is targeted than when the inner leaflet is targeted. However, taking into account the size difference between the budding and the original vesicle (typically one-fifth, as in Fig. 1), the change in volume is small compared to the change in area.

Recent publications showed that the GUV electroformation method used in these experiments can lead to a small degree of lipid peroxidation (8). The presence of peroxidized lipids in our vesicles before photosensitization should have no effect on our results as long as it is symmetric regarding the leaflet localization.

CONCLUSION

The asymmetrical shape transitions observed in photosensitized GUVs reveal changes in their membrane spontaneous curvature. These modifications are in accordance with the presence of the oxidation by-products of cleaved-lipids. Permeabilization and a decrease of lysis tension were also characterized. We developed a model linking the budding from spontaneous curvature change, to a tension of the membrane up to the lysis level, where membranes are permeated. These findings might shed a new light on some membrane permeation phenomenon involved in biomedicine photodynamic approaches and in cell oxidative stress.

APPENDIX

In this Appendix, we calculate the energy gained from budding a vesicle. The ADE model Hamiltonian is

$$H = \frac{1}{2}k_c\int (C_1 + C_2 - C_0)^2 dA + \frac{\alpha\pi k_c}{2Ah^2}(\Delta A - \Delta A_0)^2, \tag{14}$$

where C_1 and C_2 are the local curvatures of the vesicle, C_0 is the spontaneous curvature of the membrane, ΔA is the area difference between the outer and the inner leaflet, and ΔA_0 is the preferred area difference between the leaflets. Oxidation will change lipid area of the outer leaflet from A to $A + \Delta A_0$, and the spontaneous curvature of the outer membrane lipids from essentially 0 to C_0.

For a sphere of radius R,

$$H_1 = \frac{1}{2}k_c\left(\frac{2}{R} - C_0\right)^2 A + \frac{\alpha\pi k_c}{2Ah^2}(8\pi Rh - \Delta A_0)^2. \tag{15}$$

For a sphere of radius R' plus an internal bud of radius $r << R$ (we keep the total area constant so that $R'^2 + r^2 = R^2$):

$$H_2 = \frac{1}{2}k_c\left(\frac{2}{R'} - C_0\right)^2 4\pi\left(R^2 - r^2\right) + \frac{1}{2}k_c\left(\frac{2}{r} - C_0\right)^2 4\pi r^2 + \frac{\alpha\pi k_c}{2Ah^2}(8\pi R'h - 8\pi rh - \Delta A_0)^2. \tag{16}$$

Assuming $1/R << C_0$, the energy difference when budding is then

$$\begin{aligned}\Delta H &= H_2 - H_1 \\ &= \frac{1}{2}k_c 4\pi r^2\left(\left(\frac{2}{r} - C_0\right)^2 - {C_0}^2\right) + \frac{\alpha\pi k_c}{2Ah^2}\Big((8\pi R'h \\ &\quad - 8\pi rh - \Delta A_0)^2 - (8\pi Rh - \Delta A_0)^2\Big).\end{aligned} \tag{17}$$

It can be simplified as

$$\Delta H = \frac{1}{2}k_c 4\pi r^2\left(\frac{4}{r^2} - \frac{4C_0}{r}\right) - \frac{\alpha\pi k_c}{2Ah^2}16\pi rh\Delta A_0, \tag{18}$$

$$\Delta H = 8\pi k_c\left(1 - C_0 r - \frac{\alpha\pi}{h}r\frac{\Delta A_0}{A}\right), \tag{19}$$

$$\Delta H = 8\pi k_c\left(1 - C_0^* r\right), \tag{20}$$

with $C_0^* = C_0 + (\alpha\pi/h)(\Delta A_0/A)$ as the effective spontaneous curvature.

SUPPORTING MATERIAL

One figure and one movie are available at http://www.biophysj.org/biophysj/supplemental/S0006-3495(09)01457-X.

The authors thank S. Cribier for the use of her micropipette device and C. Gourier for her microforge device, and also thank R. Santus, P. Sens, N. Puff, and N. Coq for useful discussions.

REFERENCES

1. Halliwell, B. 1989. Free radicals, reactive oxygen species and human disease: a critical evaluation with special reference to atherosclerosis. *Br. J. Exp. Pathol.* 70:737–757.
2. Girotti, A. W. 1990. Photodynamic lipid peroxidation in biological systems. *Photochem. Photobiol.* 51:497–509.
3. Ross, R. 1993. The pathogenesis of atherosclerosis: a perspective for the 1990s. *Nature.* 362:801–809.
4. Cadenas, E., and L. Parcker. 1999. Understanding the Process of Aging: the Roles of Mitochondria, Free Radicals and Antioxidants. CRC Press, New York.
5. Girotti, A. W., and T. Kriska. 2004. Role of lipid hydroperoxides in photo-oxidative stress signaling. *Antioxid. Redox Signal.* 6:301–310.
6. Paillous, N., and S. Fery-Forgues. 1994. Interest of photochemical methods for induction of lipid peroxidation. *Biochimie.* 76:355–368.
7. Borst, J. W., N. V. Visser, O. Kouptsova, and A. J. Visser. 2000. Oxidation of unsaturated phospholipids in membrane bilayer mixtures is accompanied by membrane fluidity changes. *Biochim. Biophys. Acta.* 1487:61–73.
8. Ayuyan, A. G., and F. S. Cohen. 2006. Lipid peroxides promote large rafts: effects of excitation of probes in fluorescence microscopy and electrochemical reactions during vesicle formation. *Biophys. J.* 91:2172–2183.
9. Dougherty, T. J., C. J. Gomer, B. W. Henderson, G. Jori, D. Kessel, et al. 1998. Photodynamic therapy. *J. Natl. Cancer Inst.* 90:889–905.
10. Selbo, P. K., G. Sivam, O. Fodstad, K. Sandvig, and K. Berg. 2001. In vivo documentation of photochemical internalization, a novel approach to site-specific cancer therapy. *Int. J. Cancer.* 92:761–766.
11. Kuimova, M. K., G. Yahioglu, and P. R. Ogilby. 2009. Singlet oxygen in a cell: spatially dependent lifetimes and quenching rate constants. *J. Am. Chem. Soc.* 131:332–340.
12. Moan, J. 1990. On the diffusion length of singlet oxygen in cells and tissues. *J. Photochem. Photobiol.* 6:343–347.
13. Dairou, J., C. Vever-Bizet, and D. Brault. 2004. Interaction of sulfonated anionic porphyrins with HIV glycoprotein gp120: photodamages revealed by inhibition of antibody binding to V3 and C5 domains. *Antiviral Res.* 61:37–47.
14. Piette, J., C. Volanti, A. Vantieghem, J. Y. Matroule, Y. Habraken, et al. 2003. Cell death and growth arrest in response to photodynamic therapy with membrane-bound photosensitizers. *Biochem. Pharmacol.* 66:1651–1659.
15. Mojzisova, H., S. Bonneau, and D. Brault. 2007. Structural and physico-chemical determinants of the interactions of macrocyclic photosensitizers with cells. *Eur. Biophys. J.* 36:943–953.
16. Bonneau, S., and C. Vever-Bizet. 2008. Tetrapyrrole photosensitizers, determinants of subcellular localization and mechanisms of photodynamic processes in therapeutic approaches. *Expert Opin. Ther. Pat.* 18:1025–1040.
17. Bonneau, S., C. Vever-Bizet, H. Mojzisova, and D. Brault. 2007. Tetrapyrrole-photosensitizers vectorization and plasma LDL: a physicochemical approach. *Int. J. Pharm.* 344:78–87.
18. Mojzisova, H., S. Bonneau, C. Vever-Bizet, and D. Brault. 2007. The pH-dependent distribution of the photosensitizer chlorin e6 among plasma proteins and membranes: a physico-chemical approach. *Biochim. Biophys. Acta.* 1768:366–374.
19. Mojzisova, H., S. Bonneau, C. Vever-Bizet, and D. Brault. 2007. Cellular uptake and subcellular distribution of chlorin e6 as functions of pH and interactions with membranes and lipoproteins. *Biochim. Biophys. Acta.* 1768:2748–2756.
20. Hope, M. J., T. E. Redelmeier, K. F. Wong, W. Rodrigueza, and P. R. Cullis. 1989. Phospholipid asymmetry in large unilamellar vesicles induced by transmembrane pH gradients. *Biochemistry.* 28:4181–4187.
21. Farge, E., and P. F. Devaux. 1992. Shape changes of giant liposomes induced by an asymmetric transmembrane distribution of phospholipids. *Biophys. J.* 61:347–357.

22. Dobereiner, H. G., E. Evans, M. Kraus, U. Seifert, and M. Wortis. 1997. Mapping vesicle shapes into the phase diagram: a comparison of experiment and theory. *Phys. Rev. E Stat. Phys. Plasmas Fluids Relat. Interdiscip. Topics.* 55:4458–4474.

23. Nikolov, V., R. Lipowsky, and R. Dimova. 2007. Behavior of giant vesicles with anchored DNA molecules. *Biophys. J.* 92:4356–4368.

24. Petrov, P. G., J. B. Lee, and H. G. Döbereiner. 1999. Coupling chemical reactions to membrane curvature: a photochemical morphology switch. *Europhys. Lett.* 48:435–441.

25. Hamada, T., Y. T. Sato, K. Yoshikawa, and T. Nagasaki. 2005. Reversible photoswitching in a cell-sized vesicle. *Langmuir.* 21:7626–7628.

26. Helfrich, W. 1973. Elastic properties of lipid bilayers: theory and possible experiments. *Z. Naturforsch. C: Biosci.* 28:693–703.

27. Miao, L., U. Seifert, M. Wortis, and H. G. Döbereiner. 1994. Budding transitions of fluid-bilayer vesicles: the effect of area-difference elasticity. *Phys. Rev. E Stat. Phys. Plasmas Fluids Relat. Interdiscip. Topics.* 49:5389–5407.

28. Seifert, U. 1997. Configurations of fluid membranes and vesicles. *Adv. Phys.* 46:137.

29. Olbrich, K., W. Rawicz, D. Needham, and E. Evans. 2000. Water permeability and mechanical strength of polyunsaturated lipid bilayers. *Biophys. J.* 79:321–327.

30. Faure, C., F. Nallet, D. Roux, S. T. Milner, F. Gauffre, et al. 2006. Modeling leakage kinetics from multilamellar vesicles for membrane permeability determination: application to glucose. *Biophys. J.* 91:4340–4349.

31. Sandre, O., L. Moreaux, and F. Brochard-Wyart. 1999. Dynamics of transient pores in stretched vesicles. *Proc. Natl. Acad. Sci. USA.* 96:10591–10596.

32. Rodriguez, N., S. Cribier, and F. Pincet. 2006. Transition from long- to short-lived transient pores in giant vesicles in an aqueous medium. *Phys. Rev. E Stat. Nonlin. Soft Matter Phys.* 74:061902.

33. Karatekin, E., O. Sandre, H. Guitouni, N. Borghi, P. H. Puech, et al. 2003. Cascades of transient pores in giant vesicles: line tension and transport. *Biophys. J.* 84:1734–1749.

34. Idiart, M. A., and Y. Levin. 2004. Rupture of a liposomal vesicle. *Phys. Rev. E Stat. Nonlin. Soft Matter Phys.* 69:061922.

35. Angelova, M., and D. S. Dimitrov. 1988. A mechanism of liposome electroformation. *In* Trends in Colloid and Interface Science II. V. Degiorgio, editor. Springer-Verlag, Darmstadt, Germany.

36. Rodriguez, N., J. Heuvingh, F. Pincet, and S. Cribier. 2005. Indirect evidence of submicroscopic pores in giant unilamellar vesicles. *Biochim. Biophys. Acta.* 1724:281–287.

37. Zenkevich, E., E. Sagun, V. Knyukshto, A. Shulga, A. Mironov, et al. 1996. Photophysical and photochemical properties of potential porphyrin and chlorin photosensitizers for PDT. *J. Photochem. Photobiol. B.* 33:171–180.

38. Castano, A. P., T. N. Demidova, and M. R. Hamblin. 2005. Mechanisms in photodynamic therapy: part two—cellular signaling, cell metabolism and modes of cell death. *Photodiagn. Photodyn. Ther.* 2:1–23.

39. Buettner, G. R., and B. A. Jurkiewicz. 1996. Catalytic metals, ascorbate and free radicals: combinations to avoid. *Radiat. Res.* 145:532–541.

40. Buettner, G. R. 1993. The pecking order of free radicals and antioxidants: lipid peroxidation, α-tocopherol, and ascorbate. *Arch. Biochem. Biophys.* 300:535–543.

41. Domingues, M. R., A. Reis, and P. Domingues. 2008. Mass spectrometry analysis of oxidized phospholipids. *Chem. Phys. Lipids.* 156:1–12.

42. Dobereiner, H. G., E. Evans, U. Seifert, and M. Wortis. 1995. Spinodal fluctuations of budding vesicles. *Phys. Rev. Lett.* 75:3363.

43. Chang, D. C., and T. S. Reese. 1990. Changes in membrane structure induced by electroporation as revealed by rapid-freezing electron microscopy. *Biophys. J.* 58:1–12.

44. Brochard-Wyart, F., P. G. de Gennes, and O. Sandre. 2000. Transient pores in stretched vesicles: role of leak-out. *Physica A.* 278:32–51.

45. Rawicz, W., K. C. Olbrich, T. McIntosh, D. Needham, and E. Evans. 2000. Effect of chain length and unsaturation on elasticity of lipid bilayers. *Biophys. J.* 79:328–339.

46. Devaux, P. F., A. Herrmann, N. Ohlwein, and M. M. Kozlov. 2008. How lipid flippases can modulate membrane structure. *Biochim. Biophys. Acta.* 1778:1591–1600.

47. Glassinger, E., and R. M. Raphael. 2006. Influence of thermally driven surface undulations on tethers formed from bilayer membranes. *Biophys. J.* 91:619–625.